Microstructure and Strength of Al_2O_3 – EN24 Vacuum Brazed Joints

Sree Vardhan Lalam
Director General (Naval Systems & Materials), NSTL Campus, Visakhapatnam – 530 027, India

ABSTRACT

In the present investigation, microstructural features and lap shear strength of vacuum brazed joints of polycrystalline alumina and low alloy steel EN24 were investigated. The joints were brazed in vacuum brazing furnace at 850°C by varying time using Ag26.7Cu4.5Ti (wt%) brazing alloy. The microstructure was characterized by optical microscope and scanning electron microscope (SEM). Qualitative and quantitative phase analysis was carried out from SEM Energy Dispersive Spectroscopy (EDS), Electron Probe Micro Analysis (EPMA) and X-Ray Diffraction (XRD) analysis. The presence of phases TiO_2, $(Al,Ti)_2O_3$, $CuAlO_2$, $Cu_3(Ti,Al)_3O$, $Cu_2(Ti,Al)_4O$ and intermetallics of Cu-Ti were observed in the brazed joint near alumina interface; presence of Cu_3Ti, Ag-Cu hypo- and hypereutectic solid solutions and formation of FeTi and $TiFe_2$ intermetallics were observed in the brazed joint near En24 interface. The thickness of the reaction layers increased with increase in brazing time. Lap shear strength of the brazed joints increased from 56±16 MPa to 76±14 MPa with increase in brazing time from 15 minutes to 45 minutes.

Key words: Dissimilar metal brazing, vacuum brazing, active metal brazing, En24 and Al_2O_3.

1.0 INTRODUCTION

Alumina is one of the most important ceramic materials, both pure and as a ceramic and glass component [1, 2]. It is chemically very stable and unreactive, leading to applications as high-temperature components, internal combustion engines, catalyst substrates and biomedical implants. The hardness, strength, and abrasion resistance of alumina are among the highest for oxides, making it useful for tank armor plates, abrasive materials, bearings, and cutting tools. Low alloy steel En24 [3] is widely used as automobile main shafts, valves, high-duty engine connecting rods and mandrel bars. In automobile engineering there is a necessity to join these two materials to combine their characteristics. Out of the techniques developed so far for joining ceramics to ceramics/metals including brazing, diffusion bonding, microwave welding and ultrasonic welding, brazing is one of the main methods [4–6]. Due to high thermodynamic stability of alumina (ΔDG = -1582 kJ/mol at 298K and ΔG = -1034 kJ/mol at 2000K, [7]) relative to that of metals, alumina has poor wetting characteristics. This problem can be overcome by applying active filler braze materials which contain elements like Ti, Zr and V for surface activation and improving wettability [8–13]. The brazing process usually leads to formation of different reaction products in distinct layers or dispersed inside the brazing filler. The formation of such reaction products may improve the joint strength. To obtain adequate ceramic-metal joint strength, chemical phenomena controlling the interfacial reaction between ceramic and metal, microstructural features and thickness of interaction layers are to be considered [14].

In this work, microstructural features and lap shear strength of vacuum brazed dissimilar joints of polycrystalline alumina and low alloy steel En24 were investigated. Effects of brazing time on microstructure and lap shear strength were highlighted in this report.

2.0 EXPERIMENTAL PROCEDURE

2.1 Materials

High density polycrystalline alumina samples with small additives of silica and iron oxide (together < 0.1 wt%) were cut into 10mm x 10mm x 6mm sizes. Low alloy steel samples 16mm in diameter and 30mm long were prepared for brazing. Prior to cutting, En24 was austenized at 850°C for 0.5hr, quenched in oil and then tempered at 220°C for 3hrs.

Both alumina and steel samples are polished by standard metallographic methods, cleaned thoroughly in acetone and preserved in separate desiccators for brazing purpose. 100μm thick brazing alloy foils of size 12mm by 12mm were cut from the spool, cleaned thoroughly in acetone and preserved in desiccators for further use. The solidus temperature of brazing filler is 780°C and liquidus temperature is 900°C [4]. **Table 1** shows the nominal compositions of En24 and brazing filler.

Table 1: Nominal chemical composition of low alloy steel En24 and brazing filler (wt%)

	Ni	Fe	Cr	Mo	C	Ti	Cu	Ag	Others
En24	1.65	Bal.	0.7	0.2	0.38	–	–	–	0.6Mn, 0.2Si
Filler	–	–	–	–	–	4.5	26.7	Bal.	--

2.2 Brazing Details

Brazing alloy was preplaced between steel and alumina, by keeping steel in the bottom. All the samples were kept in a stainless steel fixture and loaded into the furnace. Brazing was carried out in high temperature vacuum brazing furnace in the range of 5×10^{-5} to 5×10^{-6} mbar vacuum at 850°C for 15, 30 and 45 minutes. The heating rate was controlled at 10°C/min and the average cooling rate was 10°C/min between 850°C and 500°C throughout the experiments. In each cycle, isothermal soaking for 10 minutes was given at 500°C and 700°C during heating to minimize the stresses developing due to thermal expansion mismatch between steel and alumina.

2.3 Microstructure Examination

The as-brazed joints were sectioned, mounted and polished by standard metallographic techniques. Optical microscope and SEM were used for examining microstructure, EDS analysis and fractography. XRD was taken on fractured interfaces after lap shear testing to identify the phases present. EPMA line-scans were generated for Ag, Cu, Ti, Al, O and Fe across the brazed joints. For SEM and EPMA purpose the samples were coated with Au-Pd alloy to make conductive on Al_2O_3 side.

2.4 Mechanical Testing

Lap-shear strength of the joints was evaluated by "walter+bai ag" 200 kN capacity testing machine at a crosshead speed of 0.5mm min^{-1}. Five samples were tested for each brazing condition.

3.0 RESULTS AND DISCUSSION

3.1 Microstructure

It is seen from the binary phase diagram of Ti-O, titanium can dissolve about 32 at.% of oxygen at 850°C and forms a family of oxides ranging from TiO to TiO_2 [15]. At 850°C, Ti present in the liquid filler alloy reacts with solid alumina and forms solid titanium oxides and releases Al as solute. The joining process is due to the interdiffusion of Ti, Cu and Ag from brazing alloy towards alumina and Al, O from alumina towards the filler metal, hence forms intermetallic layers at the interface. Intermetallic layers formed during brazing in the joints of alumina with Ti containing active metal brazing fillers, in general, can be classified into four layers: First layer of alumina solid solution with interdiffused Ti and Cu; Second layer consisting of oxides of titanium; Third layer of complex oxides of Cu, Ti and Al; Fourth layer a mixture of Ag rich and Cu rich solid solutions or a mixture of Ag-Cu hypo- and hypereutectic solid solutions. But the reaction products and layers thickness depends on the brazing temperature, time and Ti concentration of brazing filler [14,16,17]. The SEM BSE images of asbrazed joints are presented in **Fig. 1**. The joints were free from pores or voids and cracks. Three distinct reaction layers (L1–L3) were observed in brazed joint with brazing time 15 min, 30 min and four layers (L0–L3) were observed in 45 min brazed joint.

3.1.1 Joint microstructure after 15 min vacuum brazing

Fig. 2 represents the BSE image of 15 minutes brazed joint

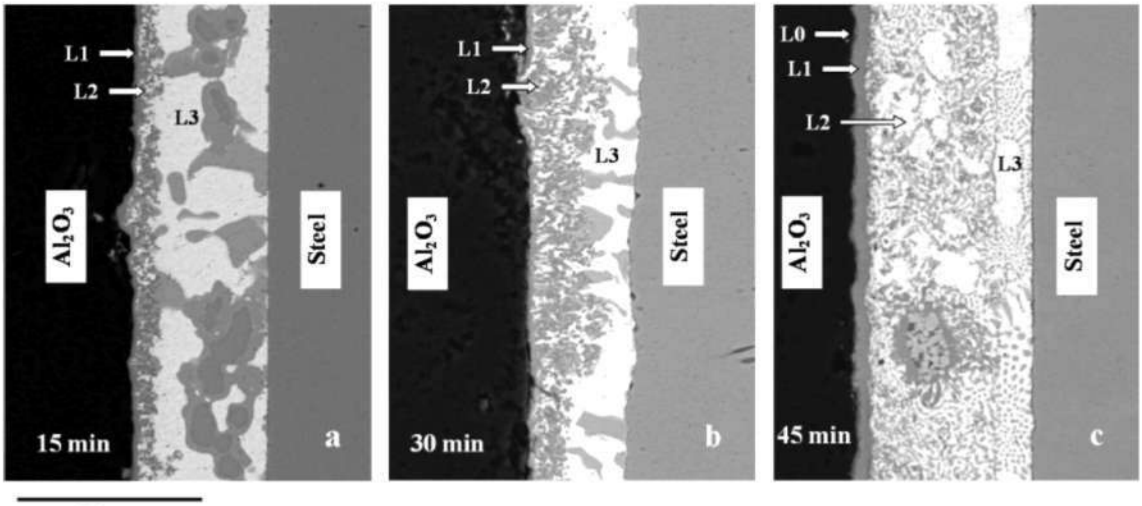

Fig. 1: SEM BSE images of alumina-steel joints vacuum brazed at 850°C for (a) 15 min (b) 30 min and (c) 45 min.

revealing the reaction layers (L1, L2 and L3) near alumina side (**Fig 2a**) and near steel side (**Fig 2b**). To identify the phases present, SEM EDS analysis was performed and the analyzed areas were marked A to F in **Fig. 2a** and A to E in **Fig. 2b**. The quantitative analysis is presented in Table 2.

The region A in **Fig. 2a** is the interface of alumina and brazing seam. SEM EDS analysis in this region shows presence of Ti and Cu due to interdiffusion. Similarly, the region A in **Fig. 2b**, the interface of steel and brazing seam shows interdiffusion of Ti and Cu into steel. Layer L1 consists of continuous dark grey coloured layer (region B in **Fig 2a**). From the atomic ratios of Cu, Ti, Al and O the phases coexisting in this region are possibly coexisting of phases $(Al,Ti)_2O_3$ and $CuAlO_2$. Layer L2 consists of mixture of three distinct phases, white coloured islands (regions C), dark coloured areas (regions D) and light grey coloured areas (regions E). The region C is Ag solid solution rich in Ti and Cu. Based on the Ti/Cu ratio, the dark area labeled as D in **Fig. 2a** is possibly Cu_4Ti_3 and the light grey area E is presumably $Cu_3(Ti,Al)_3O$ phase [18]. The area F is remnant Ag lean in Ti and Cu.

At the brazing temperature, Ti reacts with alumina and releases O and Al as solutes dissolves into the molten braze alloy. Because of high affinity for oxygen, Ti forms titanium oxide which constitutes the layer L1 at the interface. The solutes O and Al reacts with Cu, Ti and Ag in the remaining melt and forms layer L2, which constitutes mixture of complex

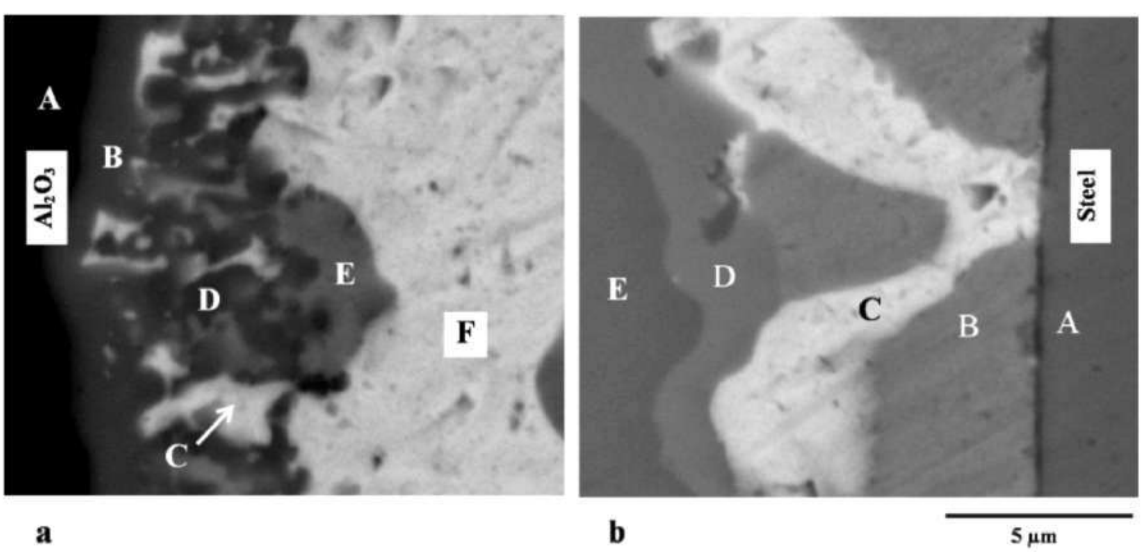

Fig. 2: SEM BSE images of 15 min brazed joint (a) alumina interface and (b) En24 interface.

oxides of Cu and Ti, intermetallic compounds of Cu–Ti. The residual brazing alloy is a primary silver solid solution with variable concentration of Ti and Cu.

From the interface of En24 and towards middle of the brazing joint, the layer L3 consists of three distinct phases (**Fig. 2b**). They are light grey coloured layer B, white coloured layer C, dark grey layer D and very dark layer E. Earlier research also well established that Ti dissolved in Cu or AgCu alloys, reacts with alumina forming at the metal-ceramic interface layers of Ti oxides or Cu-Ti-O compounds [18-22]. From the EDS quantitative analysis (**Table 2**), the layer B which in immediate contact of En24 could be a mixture of Cu solid solution and FeTi [23-24]; the region C is Ag solid solution rich in Cu; the area D is probably Cu-Ti intermetallic phase Cu_3Ti or complex oxide Cu_3TiO_5; the area E is Cu(Ti,Al). The measured thickness of layer L1 is 1.7±0.4μm and L2 is 5.1±0.9μm.

Table 2: SEM EDS analysis of phases present in 15 min brazed joint.

Region	O	Al	Ag	Ti	Fe	Cu	Possible Phase(s)
Near Al_2O_3 interface:							
B(Min)	26.1	22.6	1.6	20.4	0.7	18.2	$(Al,Ti)_2O_3$, $CuAlO_2$
(Max)	33.6	25.6	1.7	27.1	0.6	21.8	
C	0.0	4.18	58.6	8.79	1.9	9.9	Ag SS
	0.0	5.66	80.7	16.67	2.9	17.65	
D	0.0	4.5	9.4	30.1	1.4	46.3	Cu_4Ti_3
	0.0	7.1	15.1	36.2	1.7	48.2	
E	10.6	3.2	2.42	4.8	1.1	42.17	$Cu_3(Ti,Al)_3O$
	20.8	11.6	20.8	22.9	1.4	59.2	
F	0.0	1.9	75.1	0.55	2.1	6.9	Ag SS
	0.0	3.7	80.9	2.8	3.3	10.8	
Near En24 interface:							
B	6.4	3.1	4.5	3.5	2.9	76.0	Cu SS, FeTi
	6.8	3.9	4.8	4.0	5.4	79.5	
C	0.0	1.9	61.3	0.5	2.1	7.2	Ag SS
	0.0	4.2	65.2	0.7	4.0	11.1	
D	0.0	0.0	2.0	17.1	1.3	66.4	Cu_3Ti or Cu_3TiO_5
	8.8	2.8	4.9	19.0	5.3	74.5	
E	0.0	0.0	1.5	39.2	1.1	53.2	CuTi or Cu(Ti,Al)
	0.0	2.7	2.6	41.9	2.1	54.6	

3.1.2 Joint microstructure after 30 min vacuum brazing

Microstructure of 30 minutes brazed joint is shown in **Fig. 3.** SEM EDS quantitative analysis of all the regions is presented in **Table 3**. Based on analysis of atomic ratios, the region A (Fig. 3a), which is in immediate contact with alumina, possibly is a mixture of coexisting phases of $(Al,Ti)_2O_3$ and $CuAlO_2$. Region B consists of phases TiAg and Ag solid solution, region C could be $Cu_3(Al,Ti)_3O$ and region D is Cu_3Ti. At the interface of steel four different types of phases were identified (**Fig. 3b**). Region A is primary Ag solid solution rich in Cu, region B is a mixture of copper solid solution and intermetallic FeTi; region C is also copper solid solution with variation in other solute elements and the region D is Cu3Ti phase. The thickness of layers L1 and L2 are 2.1±0.4μm and 12.6±1.3μm, respectively.

Table 3: SEM EDS analysis of phases present in 30 min. brazed joint

Region	O	Al	Ag	Ti	Fe	Cu	Possible Phase(s)
Near Al_2O_3 interface:							
A(Min)	32.6	16.4	1.9	23.4	0.6	21.7	$(Al,Ti)_2O_3$, $CuAlO_2$
(Max)	35.5	18.7	2.5	24.5	0.7	22.5	
B	0.0	2.5	28.1	23.4	1.7	16.7	TiAg, Ag SS
	5.5	3.5	54.7	29.0	1.9	33.0	
C	7.7	0.0	3.9	31.6	1.2	39.2	$Cu_3(Ti,Al)_3O$
	12.6	4.1	13.3	38.9	1.8	46.0	
D	4.3	3.6	3.4	10.9	0.9	60.7	Cu_3Ti
	9.6	3.9	5.8	20.5	1.6	76.4	
Near En24 interface:							
A	0.0	0.0	77.9	0.7	3.6	10.4	Ag SS
	0.0	5.1	84.5	1.4	5.2	12.2	
B	5.0	2.3	5.2	3.1	2.6	68.4	Cu SS, FeTi
	10.4	2.8	6.4	6.3	8.4	77.7	
C	4.6	1.3	3.1	3.4	1.3	78.8	Cu SS
	7.6	3.0	7.0	5.1	2.8	82.2	
D	3.9	0.0	2.3	14.0	0.9	69.4	Cu_3Ti
	6.6	3.1	2.7	19.2	6.8	72.3	

3.1.3 Joint microstructure after 45 min vacuum brazing

Microstructure of 45 minutes brazed joint is shown in **Fig. 4**. SEM EDS quantitative analysis of all the regions is presented in **Table 4**. A thin layer of TiO_2 (region A in **Fig. 4a**) of 1μm thickness is observed in immediate contact with alumina after brazing for 45 minutes. At brazing temperatures, initially Ti reduces alumina to Al and forms TiO and with further increase in brazing time, the titanium activity falls down at the interface and Ti_2O_3 forms from TiO. With further fall in Ti activity with increase in brazing time Ti_3O_5 then Ti_4O_7 forms and ultimately TiO2 will form at the interface. The activity of Ti reduces due to formation of titanium oxides and complex oxides of Cu, Ti and Al between alumina and molten filler interface. These phases hinder the diffusion of Ti from molten melt towards the alumina interface. A well-developed layer (region B in Fig. 4a) of $CuTi/Cu_2(Al,Ti)_4O$ is observed next to TiO_2 layer [22]. The analysis Cu/Ti ratio of region C, confirms formation of CuTi or TixOy type phases. The regions D and E are hyper- and hypoeutectic Ag-Cu solid solutions, respectively. The discontinuous islands of regions A at the steel interface (Fig. 4b) could be $Cu_3Ti/FeTi$; regions C are hypoeutectic Ag-Cu solid solution. The dark colour banded region which is separating layer L2 and L3 near En24 interface **(Fig. 4b)** is $TiFe_2$.

3.1.4 Evolution of microstructure

Evolution of microstructure of the brazing joint can be summarized as follows. At the brazing temperature, the molten filler in contact with alumina forms $(Al,Ti)_2O_3$ and Cu reacts with Al, O and forms $CuAlO_2$. With increase in brazing time, TiO_2 forms and $Cu_2(Al,Ti)_4O$ layer grows next to it. Layers of L0 and L1 constitute these phases. The next layer L2 is a mixture of intermetallics of Cu-Ti, TiAg, $Cu_3(Al,Ti)_3O$ and Ag/Cu rich solid solutions

From **Fig. 1** it is evident that the layers L1 and L2 grow with increase in brazing time. The growth of these layers is from interface of alumina towards inside of the brazing seam. Layer L3 is basically a remnant of molten filler alloy and forms intermetallics of Cu-Ti and Ag- or Cu rich solid solutions. In 15 min brazing cycle, the solidification of the remnant brazing filler is in the form of coarse islands of CuTi surrounded by Cu_3Ti phase which are in turn surrounded by either Cu or Ag solid solution. In 30 min brazing cycle, the solidification pattern of phases is similar to 15 min cycle, except major volume fraction of Ag solid solution is migrated towards low alloy steel interface (**Fig. 1b**). With further increase in brazing time, thickness of layer L2 increased to 33μm from 1μm (in 15 min cycle). Increase in brazing time facilitated the formation of eutectic microstructure along with Cu-Ti intermetallics (**Fig. 1c**). This is because of increase of Cu dissolution in the presence of Ti, as the interactions of Cu-Ti are strong compared to Ag-Ti and Cu-Ag. The findings are in good agreement with earlier reports [18-26]. The layer L3 in 45 minutes brazed sample is a mixture of Cu_3Ti, FeTi, $TiFe_2$ along with Ag rich and Cu rich solid solutions. The layer L3 is distinctly separated from layer L2 by thin layer of $TiFe_2$ phase and Cu rich Ag-Cu hypereutectic solid solution (regions B in **Fig. 4b**).

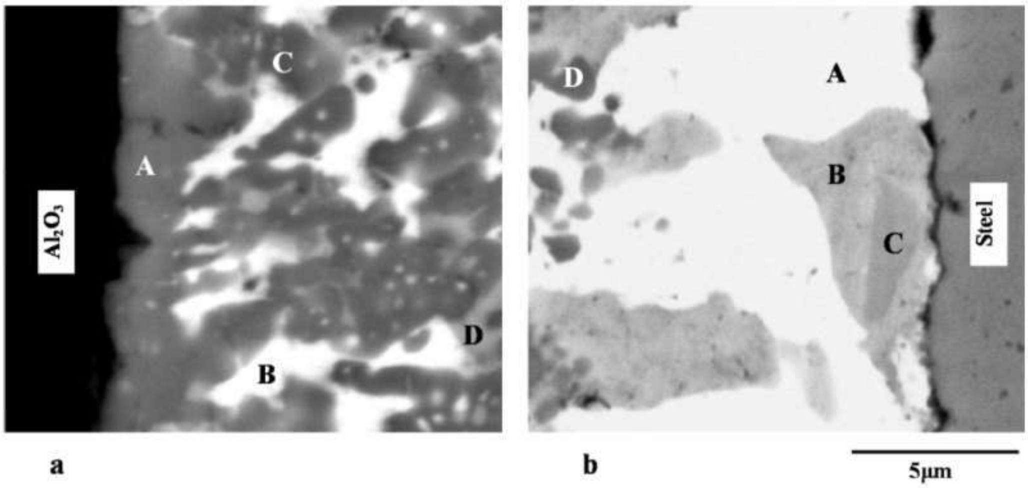

Fig. 3: SEM BSE images of 30 min brazed joint (a) alumina interface and (b) En24 interface.

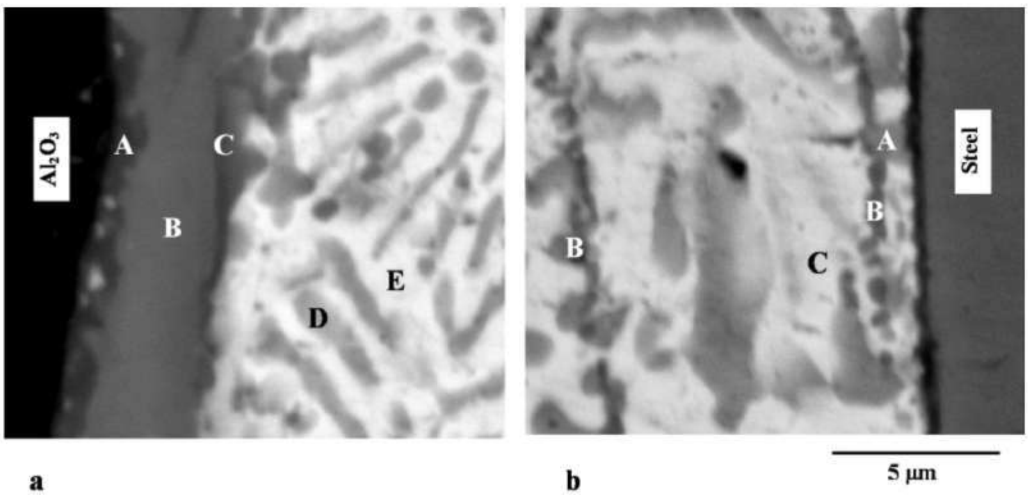

Fig. 4: SEM BSE images of 45 min brazed joint (a) alumina interface and (b) En24 interface

Table 4: SEM EDS analysis of phases present in 45 min. brazed joint.

Region	O	Al	Ag	Ti	Fe	Cu	Possible Phase(s)
Near Al_2O_3 interface:							
A(Min)	33.5	22.4	0.5	19.1	0.5	13.2	TiO_2, $(Al,Ti)_2O_3$
(Max)	40.7	28.6	1.0	25.6	0.7	16.8	
B	13.7	7.3	0.6	34.8	0.9	30.9	CuTi, $Cu_2(Ti,Al)_4O$
	25.1	9.3	1.8	40.2	1.1	36.5	
C	11.7	2.6	3.4	30.1	1.1	32.3	Ti_xO_y, CuTi
	21.0	5.4	12.4	39.9	1.3	38.1	
D	0.0	2.5	19.1	1.7	0.9	50.2	Ag-Cu Hypereutectic SS
	20.1	4.3	35.1	5.5	1.6	57.7	
E	0.0	2.4	49.6	2.3	1.8	17.1	Ag-Cu Hypoeutectic SS
	13.3	4.8	67.8	8.9	2.9	27.3	
Near En24 interface:							
A	3.1	1.2	10.9	14.7	12.3	43.1	Cu_3Ti, FeTi
	10.1	3.3	16.1	21.7	14.8	48.7	
B	4.6	0.7	27.7	0.7	2.5	59.1	Ag-Cu Hypereutectic SS,
	8.6	2.0	28.6	1.2	2.9	61.7	$TiFe_2$
C	0.0	0.0	60.1	4.6	5.6	20.1	Ag-Cu Hypoeutectic SS
	0.0	0.0	64.2	6.5	8.3	24.1	

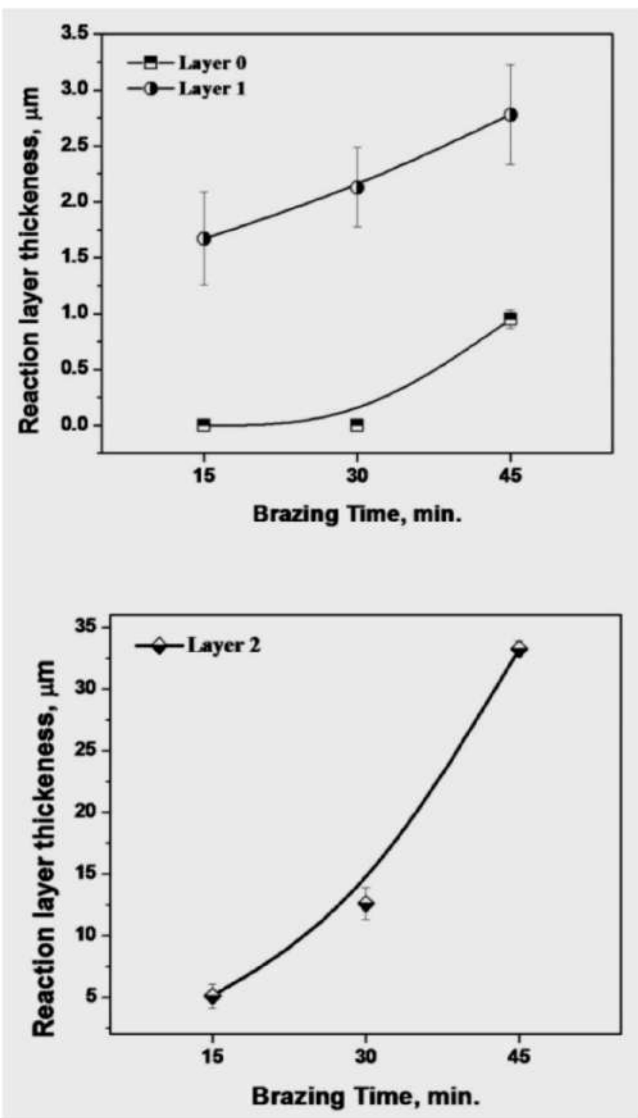

Fig. 5: Variation of reaction layers thickness with respect to brazing time.

From the microstructural analysis it is evident that in all the joints, Cu-Ti intermetallics form during brazing and the solid solutions form during cooling from 850°C to 780°C. Similar observations were also reported by Barrena et al., [27] during investigation of Al_2O_3/Ti6Al4V diffusion bond joints at 750°C, using Ag-Cu interlayer. **Fig. 5** shows the variation of all the reaction layers with respect to the brazing time. It is found that width of layer L1 increased linearly and layer L3 shown parabolic growth with increase in brazing time. Similar layer growth characteristics also were recorded by Elrefaey and Tillmann [28] during the investigation of brazing of CP Ti using Ag-Cu-In-Ti filler alloy.

3.2 EPMA line scans of brazed joints

EPMA line scans of brazed joints are shown in **Fig. 6** to **Fig. 8**. The scanning was carried out along the line marked between points 1 and 2 across the brazed joints. The line maps show the X-ray intensity versus distance for the major elements Ag, Cu and Ti. From the observation of intensity profile of Ag, the segregation of Ag is high at the interfaces of both materials in 15 min brazing cycle. The variation in intensity of Ag at the Al_2O_3 interface is due to formation of oxides of Ti, but there is no offset in rise of concentration is observed from either Al_2O_3

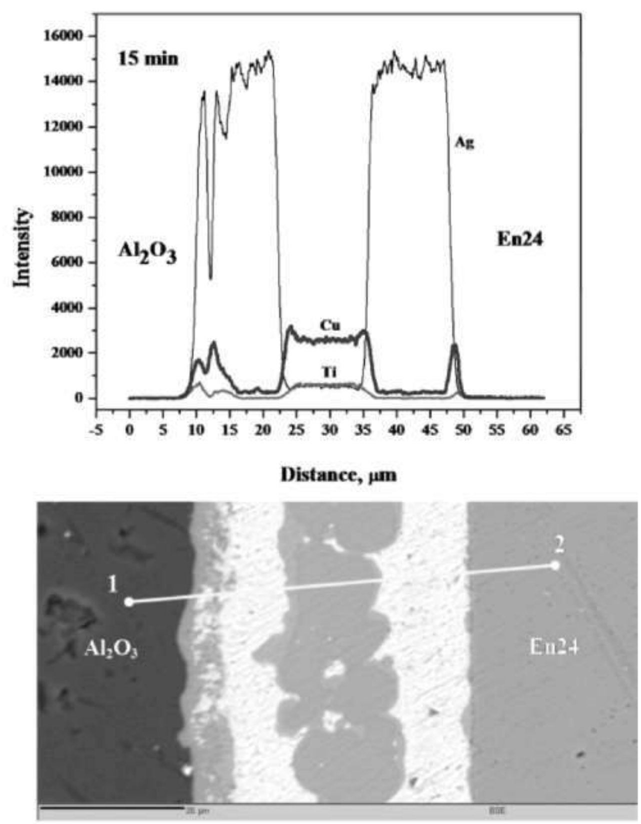

Fig. 6: EPMA X-ray intensity line map of 15 min brazed joint.

interface or En24 interface. This is because there is no pronounced growth of oxides layer at Al_2O_3 interface or intermetallics formation at En24 interface. An offset of 7~10μm is observed in 30 min brazing cycle due to formation of these phases at both the interfaces (**Fig. 1b**). It is also observed in 45 min brazed cycle, at the Al_2O_3 interface. Since formation fine banded Ag-Cu eutectic structure, offset is not observed on En24 side in 45 min brazed cycle (**Fig. 1c**).

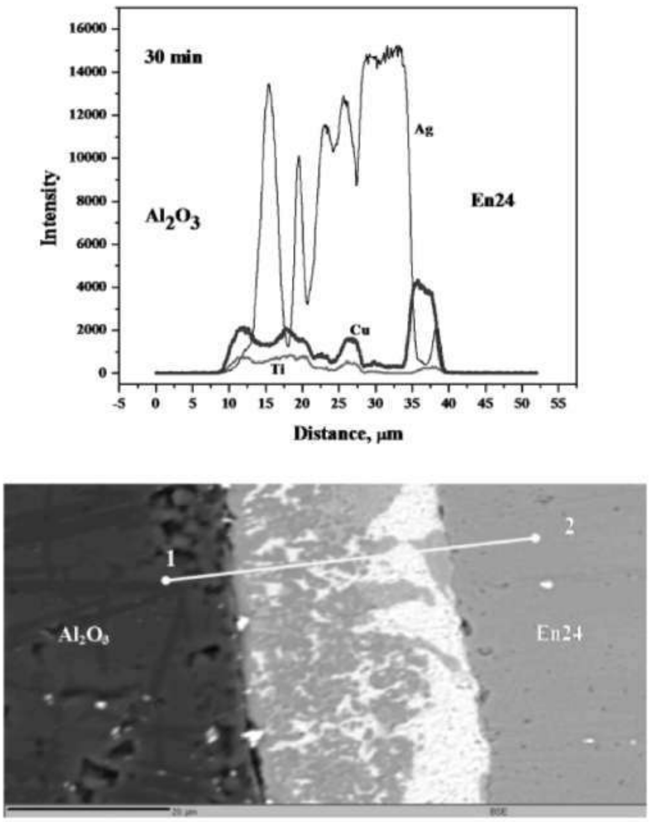

Fig. 7: EPMA X-ray intensity line map of 30 min brazed joint.

The presence of Cu and Ti at Al_2O_3 interface in the line profiles confirms the formation of Ti_xO_y type oxides and $Cu_x(Al,Ti)_yO_z$ oxides (Table 2, 3 and 4). The increase in oxygen content at the interface with brazing time (**Fig. 9**) also confirms that the formation of titanium oxide. Initially it is of TixOy type and with increase in brazing time, transforms to TiO2 (Table 4).

3.3 Lap Shear Strength

Lap shear strengths of as-brazed joints are presented in **Fig. 10.** Shear strengths of 56±16 MPa, 61±18 MPa and 76±14 MPa were achieved for 15min, 30 min and 45 min brazing time, respectively. Shear strength has increased with increase in brazing time and from the plot it is observed that the scatter is

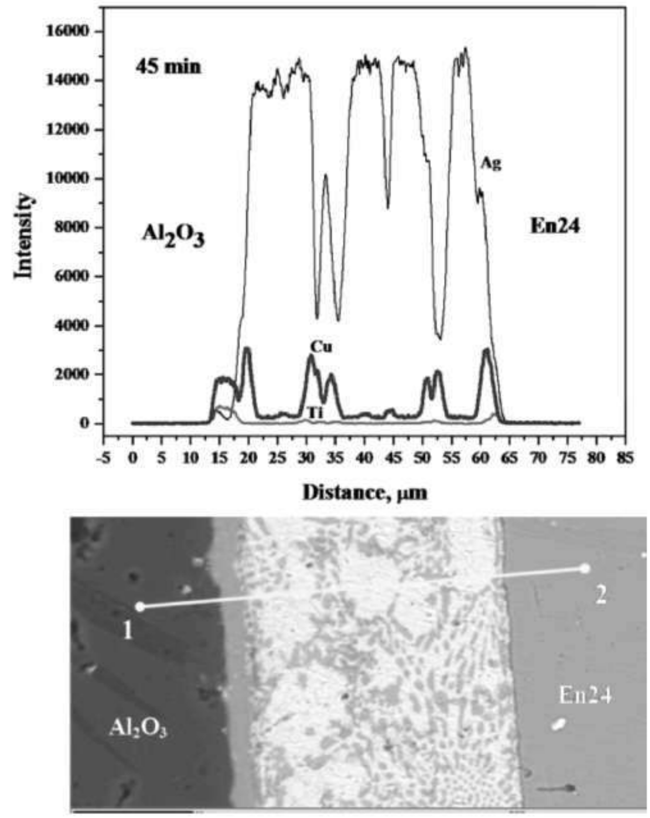

Fig. 8: EPMA X-ray intensity line map of 45 min brazed joint.

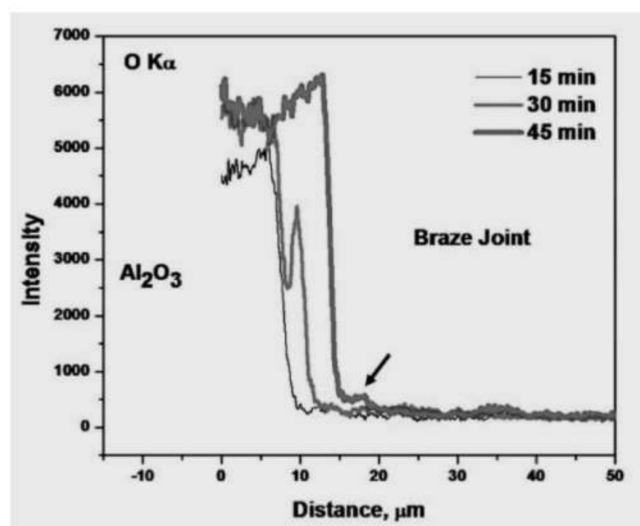

Fig. 9: Variation of O with respect to brazing time at Al_2O_3 interface.

less for 45 min brazing cycle. Some authors have reported that the shear strength increases with increase in thickness of intermetallic layers and few other authors reported that the shear strength decreases with increase in thickness of intermetallic layers [29–31]. In this present study, with

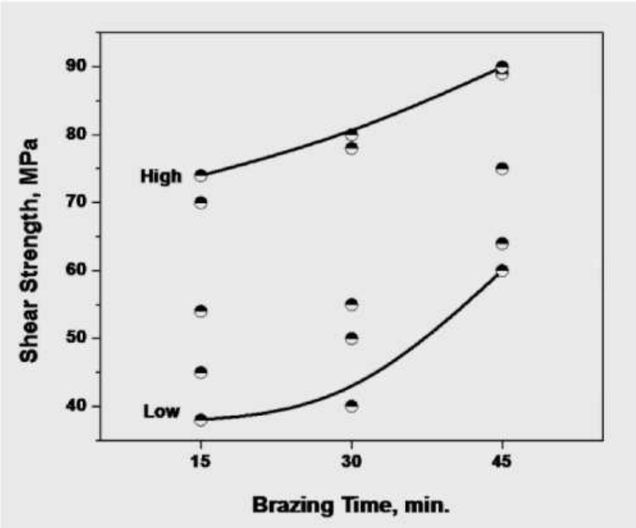

Fig. 10: Variation of lap shear strength with respect to brazing time.

increase in brazing time, reaction layer thickness increased and thickness of remnant filler alloy decreased. The maximum strength cannot be attributed to neither to variation thickness of intermetallic/complex oxides nor to remnant filler alloy. The strength, brittleness and thermal mismatch of the intermetallics and volume fraction of complex oxides are to be compensated by appropriate volume fraction of ductile cushioning remnant filler alloy.

3.4 XRD Analysis of fracture surface

The fractured surfaces were examined by XRD for phase analysis and the XRD results are shown in **Fig. 11** through **Fig. 13**. The XRD pattern of 15 min. brazing cycle (**Fig. 11**) shows maximum peaks of Al_2O_3 and the analysis also reveals the formation of titanium oxides TiO_2 and Ti_2O_3. The observations confirm that long brazing timings are not required for transformation of initially formed TiO to form higher oxides. But their volume fraction will be less for smaller brazing cycles and will increase with increase in brazing time.

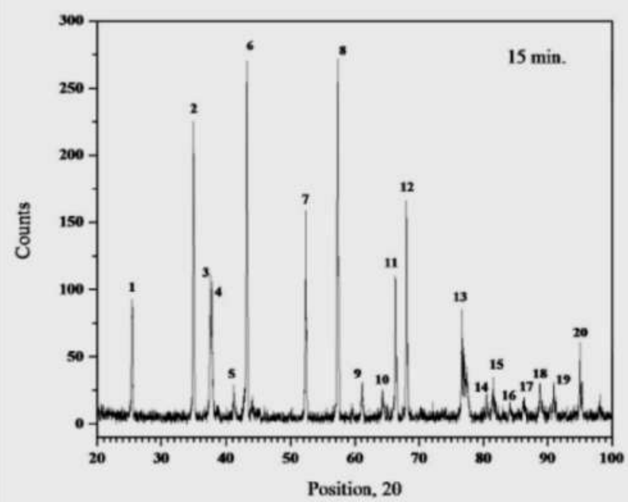

Possible phase(s)	Peak No.
Al_2O_3	1, 3, 4, 8, 9, 11, 12, 13, 14, 16, 17, 18, 19, 20
Fe_2TiO_4	2, 7
Cu_3TiO_5	2, 3
$CuAlO_2$	4, 8
TiO_2	4, 20
CuTi	5, 18
Ti_2O_3	6
TiAg	10
Ag_2O	15

Fig. 11: XRD Analysis of 15 min brazed joint.

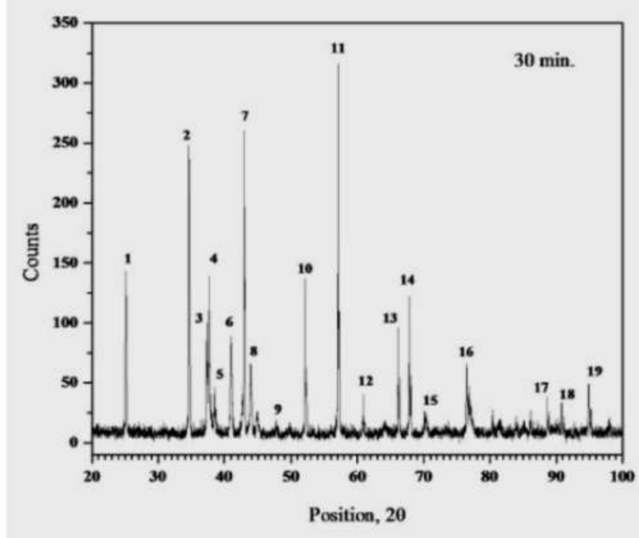

Possible phase(s)	Peak No.
Al_2O_3	3
Al_2TiO_5	2, 6
Cu_3TiO_5	4, 5, 9, 12, 15, 18
$CuAlO_2$	4, 11, 13, 14
TiO_2	1, 4, 5, 15, 19
CuTi	6, 8, 17
Ti_2O_3	2, 7, 16
Ag_2O	10

Fig. 12: XRD Analysis of 30 min brazed joint.

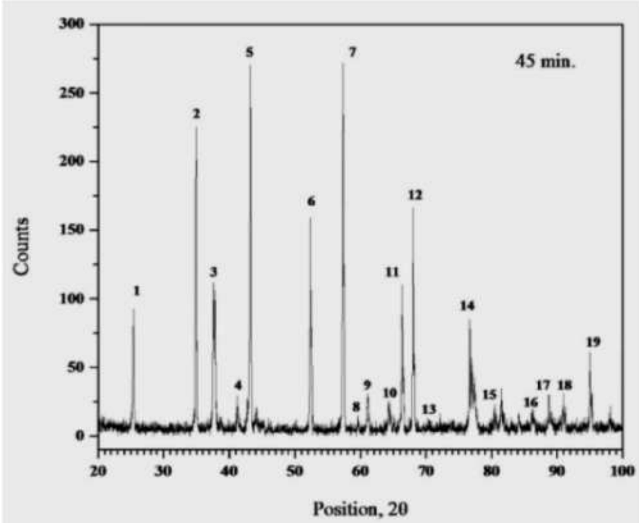

Possible phase(s)	Peak No.
Al_2O_3	1, 2, 3, 6, 7, 9, 11, 12, 13, 14, 15, 16, 17
Cu_3TiO_5	2, 3, 9, 13, 18, 19
Cu_2TiO_3	5, 9, 13
TiO_2	7, 9, 12, 14, 15, 19
Cu_4Ti_3	4, 5, 8, 14, 15
Ti_2O_3	2, 14, 17
AgO	4, 6, 8, 10, 11, 12, 16, 17, 19

Fig. 13: XRD Analysis of 45 min brazed joint.

The XRD analysis confirms formation phases Fe_2TiO_4, Cu_3TiO_5, $CuAlO_2$, CuTi, TiAg and Ag_2O. Only some of these phases are rightly identified through SEM EDS analysis of the brazed joints, as the reported chemical compositions of the complex oxides and intermetallic phases are varied over a range of concentrations. The XRD peak analysis of 30 min sample (**Fig. 12**) shows the formation larger volume fraction of complex oxides Cu_3TiO_5, $CuAlO_2$ and oxides TiO_2 and Ti_2O_3. Oxide of silver Ag_2O and CuTi are observed in both 15 and 30 min. cycle. Analysis of 45 min sample (**Fig. 13**) also confirms the increase in the volume fraction of complex oxides Cu_3TiO_5, Cu_2TiO_3 and titanium oxides TiO_2 and Ti_2O_3. Oxide of silver AgO and Cu_4Ti_3 intermetallics are also identified in XRD patterns.

3.5 Fractography

After shear testing the fractured surfaces were observed under optical microscope and SEM to study the fracture features and to identify the phases. **Fig. 14** represents the optical images of the fractured surfaces and **Fig. 15** shows the SEM image of the fracture surface area marked in **Fig. 14a**. It confirms that the fracture was initiated in the interface near to the alumina and once the area of cross section reduces to a certain level, the final fracture occurred by brittle fracture mode in alumina. EDS analysis was performed at three major areas over the fractured surfaces to identify the phases through which fracture had occurred. The areas similar to region A in **Fig. 15**, are mixture of $(Al,Ti)_2O_3$ (dark colour) and $CuAlO_2$ (grey colour); the region B is Al_2O_3 (dark colour) and region C is Ag solid solution (white colour).

4.0 CONCLUSIONS

Vacuum brazing was successfully performed between low alloy steel En24 and polycrystalline high density alumina using Ag26.7Cu4.5Ti (wt%) brazing alloy at 850°C. Microstructures showed formation of three reaction layers for 15 and 30 min brazing time; four layers for 45 min brazing time. First reaction layer next to alumina contains $(Al,Ti)_2O_3$, TiO_2 and Ti_2O_3. Second reaction layer consist of complex oxides of Cu, Al and Ti of type Cu_3TiO_5, $CuAlO_2$ and Cu_2TiO_3. Third and fourth reaction

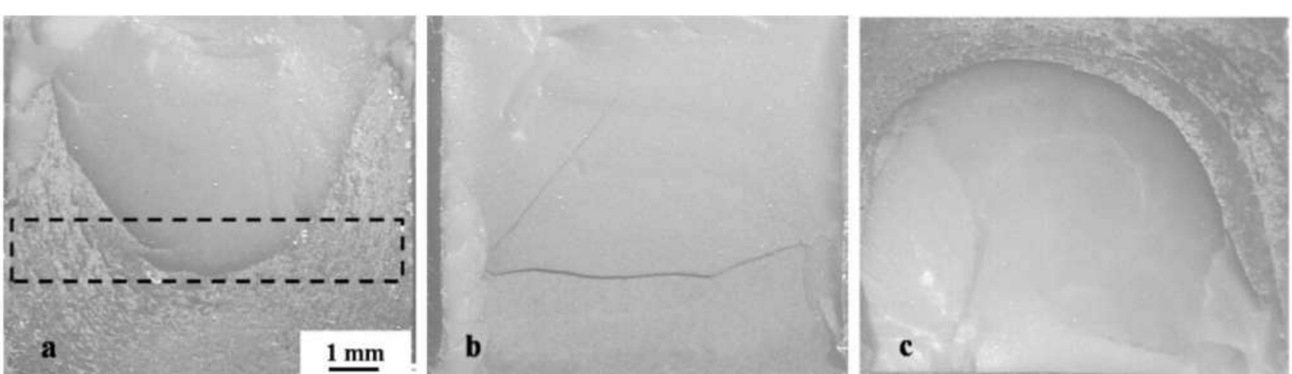

Fig. 14: Optical images of fractured surfaces of joints brazed at 850°C for (a) 15 min (b) 30 min and (c) 45 min.

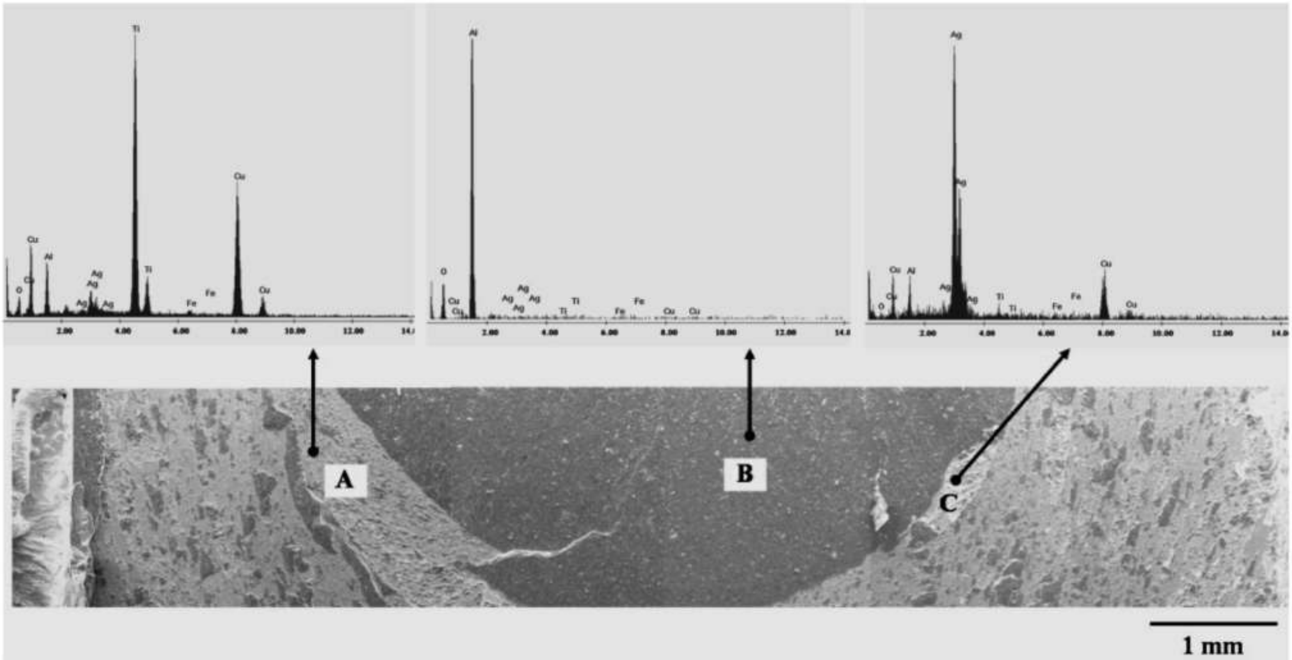

Fig. 15: SEM image of fractured surface of joint brazed for 15 min. EDS analysis of three major regions: A – $(Al,Ti)_2O_3$, $CuAlO_2$; B – Al_2O_3; C – Ag solid solution.

layers are basically remnant filler alloy with intermetallics of Cu-Ti of type CuTi and Cu_4Ti_3 with Ag-Cu hypo- and hypereutectic solid solutions containing FeTi, $TiFe_2$ intermetallic phases. Thickness of second reaction layer increased linearly and third reaction layer increased in a parabolic method with increase in brazing time. Shear strength is also increased with increase in brazing time in a parabolic manner. Failure had occurred in intermetallic layers near to alumina substrate and XRD analysis of the fracture surfaces reveal that the incubation time is not required for transformation of TiO into higher oxides of titanium at the interface of alumina.

ACKNOWLEDGEMENTS

The financial assistance from the Defence Research and Development Organization (DRDO) is gratefully acknowledged. The author would like to thank Dr. V. Bhujanga Rao, Director General (NS&M) and Dr. Amol A Gokhale, Director, Defence Metallurgical Research Laboratory (DMRL) for their continued encouragement and permission to publish this work.

REFERENCES

1. Robert H. Doremus. Alumina. In: James F. Shackelford and Robert H. Doremus, editors. Ceramic and Glass Materials -Structure, Properties and Processing, Springer Science + Business Media, LLC; 2008, p. 1-26.
2. Gitzen WH. Alumina as a Ceramic Material, The American Ceramic Society, Westerville, OH,1970.
3. The Mechanical and Physical Properties of the British Standard En Steels, Vol 2; 1966.
4. Nicholas MG. Joining of ceramics, The Institute of Ceramics, Chapman and Hall; 1990.
5. Schwartz M. Ceramic Joining. ASM International, Materials Park, OH, 1990.
6. Do Nascimento RM, Marinelli AE and Buschinelli AJA. Recent advances in metal-ceramic brazing. Ceramica 2003; 49: p. 178 – 198.
7. Ihsan Barin. Therrnochernical Data of Pure Substances. 3rd ed. VCH Verlagsgesellschaft GmbH, D-6945 1 Weinheim (Federal Republic of Germany); 1995, p. 48.
8. Naka M., et al. Trans JWRI 1983; 12(1): p. 145 – 148.
9. Chai JH, Weng WP and Chuang TH. Ceram Int 1998; 24: p. 273 – 279.

10. Mandal S, Ray AK and Ray AK. J Mat Sci Eng A 2004; 383: p. 235.

11. Paulasto M and Kivilahti J. J Mat Res 1988; 13: p. 343.

12. Vianco PT, Stephens JJ, Hlava PF and Walker CA. Weld J 2003; p. 268.

13. Weng WP, Wu HW and Chai YH. J Adv Mat 1997; 28(2): p. 35 – 40.

14. Hua Lu, Bao CL and Shen DH. J Mat Sci 1995; 30: p. 339 – 346.

15. ASM Handbook. Vol 3. Alloy Phase Diagrams. ASM International. ; p. 2.324

16. Hosking FM, Cadden CH, Yang NYC, Glass SJ, Stephens JJ, Vianco PT and Walker CA. Weld J 2000; Aug: p. 222s – 230s.

17. Kozlova O, Braccini M, Voytovych R, Eustathopoulos N, Martinetti P and Devismes MF. Acta Mat 2010; 58: p.1252 – 1260.

18. Loehman RE and Tomsia AP. Acta Mater 1994; 40: p. 547.

19. Shiue R, Wu S, O JM, Wnag JY. J Metall Mater Trans A 2000; 31; p. 2527.

20. Paulasto M, Kivilahti J. J Mater Res. 1998; 13; p. 343.

21. Carim A. Scripta Metall Mater. 1991; 25; p. 51.

22. Voytovych R, Robaut F and Eustathopoulos. Acta Mater 2006; 54; p. 2205-2214.

23. Ghosh M and Chatterjee S. Mater Char. 2002; 48; p. 393-399.

24. Noda T, Shimizu T, Okabe M and Iikubo T. Mat Sci and Eng A 1997; A239; p. 613-618.

25. Liu HB, Zhang LX, Wu LZ, Liu D and Feng JC. Mat Sci Eng A 2008; 498: p. 321-326.

26. Hultgren R et al. Selected values of thermodynamic properties of binary alloys. Metals Park, OH, ASM International 1973.

27. Barrena MI, Matesanz L and Gomez de Salazar. Mat Char. 2009.

28. Elrefaey A and Tillmann W. J Mat Proc Tech 2009.

29. Palit D and Meier AM. J Mat Sci 2006; 41: p. 7197.

30. Xong HP, Bo Chen, Kang YS, Mao W, Kawasaki A and Watanabe HR. Scripta Mat 2007; 56: p. 173.

31. Kar A, Mandal S, Ghosh RN, Ghosh TK and Ray AK. J Mat Sci 2007; 42(14): p. 5556 – 5561.